Published OnlineFirst January 22, 2021; DOI: 10.1158/0008-5472.CAN-20-1785

The Irradiated Brain Microenvironment Supports Glioma Stemness and Survival via Astrocyte-Derived Transglutaminase 2

Tracy J. Berg[1], Carolina Marques[2], Vasiliki Pantazopoulou[1], Elinn Johansson[1], Kristoffer von Stedingk[3,4], David Lindgren[1], Pauline Jeannot[1], Elin J. Pietras[5], Tobias Bergström[6], Fredrik J. Swartling[6], Valeria Governa[7], Johan Bengzon[8], Mattias Belting[6,7], Håkan Axelson[1], Massimo Squatrito[2], and Alexander Pietras[1]

ABSTRACT

The tumor microenvironment plays an essential role in supporting glioma stemness and radioresistance. Following radiotherapy, recurrent gliomas form in an irradiated microenvironment. Here we report that astrocytes, when pre-irradiated, increase stemness and survival of cocultured glioma cells. Tumor-naïve brains increased reactive astrocytes in response to radiation, and mice subjected to radiation prior to implantation of glioma cells developed more aggressive tumors. Extracellular matrix derived from irradiated astrocytes were found to be a major driver of this phenotype and astrocyte-derived transglutaminase 2 (TGM2) was identified as a promoter of glioma stemness and radioresistance. TGM2 levels increased after radiation *in vivo* and in recurrent human glioma, and TGM2 inhibitors abrogated glioma stemness and survival. These data suggest that irradiation of the brain results in the formation of a tumor-supportive microenvironment. Therapeutic targeting of radiation-induced, astrocyte-derived extracellular matrix proteins may enhance the efficacy of standard-of-care radiotherapy by reducing stemness in glioma.

Significance: These findings presented here indicate that radiotherapy can result in a tumor-supportive microenvironment, the targeting of which may be necessary to overcome tumor cell therapeutic resistance and recurrence.

Graphical Abstract: http://cancerres.aacrjournals.org/content/canres/81/8/2101/F1.large.jpg.

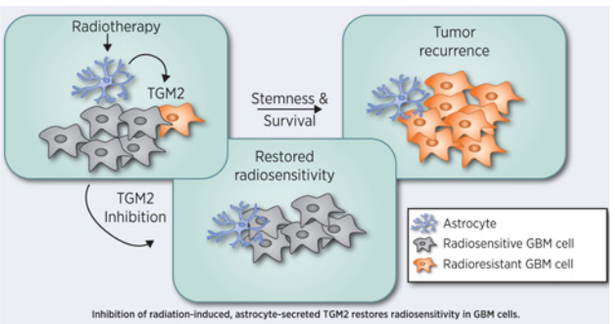

Introduction

Glioblastoma (GBM) is the most aggressive and most common glioma, with less than a 10% 5-year survival rate (1). GBM is treated by surgery, radiation, and chemotherapy, yet nearly all tumors recur (2). Recurrent tumors generally form within or overlapping the original tumor volume (3) and within a gliotic region corresponding to the initial field receiving radiation, suggesting that recurring tumors form within the irradiated microenvironment. Recurred tumors have limited treatment options.

GBM recurrence is often attributed to radioresistant glioma cells, a phenotype that is related to stemness, in that tumor cells surviving radiotherapy display characteristics of stem cells, like enhanced self-renewal and increased drug-efflux capabilities, as compared with radiation-sensitive cells (4, 5). Understanding which factors promote treatment resistance of glioma cells is of intense interest. Microenvironmental cues such as hypoxia (6), extracellular matrix proteins (7, 8), or growth factors secreted by stromal cells (9, 10) may be sufficient to induce tumor cell therapeutic resistance. Microenvironmental regulation of stemness is further supported by the finding that stem-like tumor cells are enriched in specific niches, primarily the perivascular niche and hypoxic compartments (6, 11, 12). These niches contain a variety of stromal cell types including astrocytes, microglia, endothelial cells, and pericytes (13), which contribute to glioma aggressiveness (14, 15); however, little is known about how these cells respond to radiotherapy. We sought to determine whether irradiation of the brain tumor microenvironment affects the therapeutic response of glioma cells. We identified astrocyte-derived transglutaminase 2 (TGM2) as a potential radiation-induced modifier of the tumor microenvironment, which protected against radiation-induced cell death, and may serve as a potential therapeutic target.

[1]Division of Translational Cancer Research, Department of Laboratory Medicine, Lund University, Lund, Sweden. [2]Seve Ballesteros Foundation Brain Tumor group, CNIO, Madrid, Spain. [3]Department of Pediatrics, Clinical Sciences Lund, Lund University, Lund, Sweden. [4]Department of Oncogenomics, M1–131 Academic Medical Center University of Amsterdam, Amsterdam, the Netherlands. [5]Biotech Research and Innovation Centre, University of Copenhagen, Copenhagen, Denmark. [6]Department of Immunology, Genetics and Pathology, Science for Life Laboratory, Uppsala University, Uppsala, Sweden. [7]Division of Oncology and Pathology, Department of Clinical Sciences, Lund, Lund University, Lund, Sweden. [8]Division of Neurosurgery, Department of Clinical Sciences, Lund Stem Cell Center, Lund University, Lund, Sweden.

Note: Supplementary data for this article are available at Cancer Research Online (http://cancerres.aacrjournals.org/).

Corresponding Author: Alexander Pietras, Department of Laboratory Medicine in Lund, Lund University, Medicon Village 404:C3, Lund 22363, Sweden. Phone: 46-46-2226431; E-mail: Alexander.Pietras@med.lu.se

Cancer Res 2021;81:2101–15

doi: 10.1158/0008-5472.CAN-20-1785

Published OnlineFirst January 22, 2021; DOI: 10.1158/0008-5472.CAN-20-1785

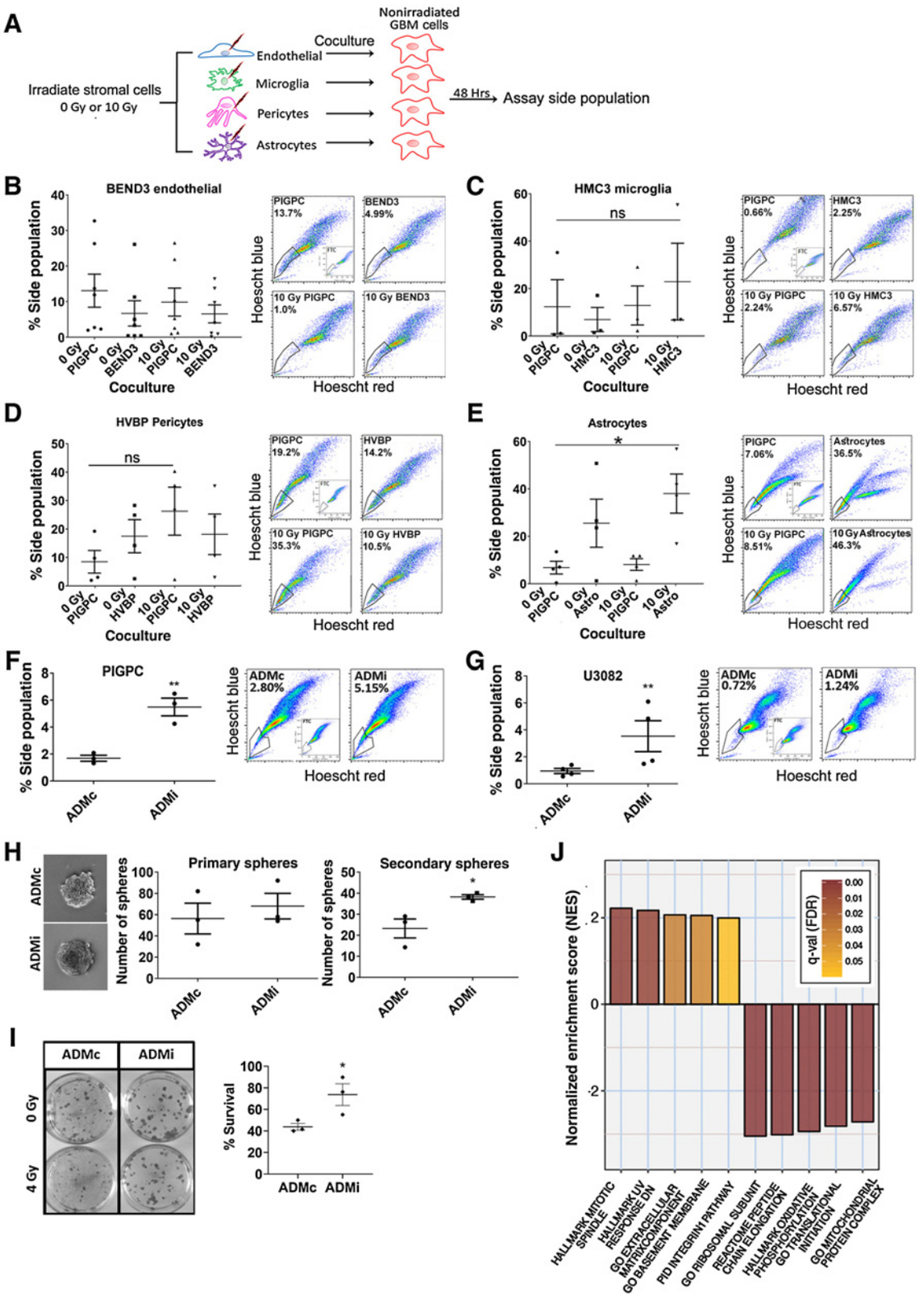

Published OnlineFirst January 22, 2021; DOI: 10.1158/0008-5472.CAN-20-1785

Materials and Methods

Mice

Figure 2A–E: B6 (RRID: IMSR_TAC:b6) mice were irradiated 1 × 10 Gy. **Figure 2F–L:** Mice were irradiated with 0–10 Gy, injected 72 hours later with PIGPC intracranially, then euthanized upon glioma symptoms. **Figures 3A–D**, **4E–I**, **5G** and **H**, **6D–F**: Male and female *Nestin-tv-a* mice (RRID: IMSR_NCIMR:01XH4) were injected with DF-1 cells (ATCC RRID:CVCL_0570) expressing RCAS-*PDGFB* and RCAS-shp53 (16, 17). Upon symptoms, mice were treated with 0–10 Gy radiation and euthanized 72 hours posttreatment. **Figure 7A–C**: *Nestin-tv-a Ink4a/Arf*$^{-/-}$ mice were injected with DF-1 cells (ATCC) expressing RCAS-*PDGFB* and RCAS-shp53. Mice were euthanized upon glioma symptoms. **Figure 7D–G**: *Nestin-tv-a* mice were injected with DF-1 cells expressing RCAS-*PDGFB* and RCAS-shPTEN. Upon glioma symptoms, mice were euthanized for primary tumors or treated daily 5 × 2 Gy and euthanized upon symptom recurrence. Laboratory animal use was conducted in accordance with European Union directive on the subject of animal rights and approved by local ethical committees CEIyBA (CBA PA37_2013)/(IACUC 029–2013/001; CNIO), M-186/14 (Lund), and 5.8.18–16350/2017 (Uppsala). Animals were distributed randomly by weight and sex into treatment groups.

Cells

PIGPC were isolated as described previously (7). PIGPC and U251 (Sigma; RRID:CVCL_0021) cells were cultured in DMEM (Corning) supplemented with 10% FBS (Biological Industries) and 1% PenStrep (Corning). HBVP (ScienCell) were cultured in PM (ScienCell) on 2 μg/cm^2 poly-l-lysine mol wt 70,000 to 150,000 (Sigma) coated plastic and used below passage 4. HMC3 (ATCC, CRL-3304, RRID:CVCL_II76) were cultured in DMEM (Corning) supplemented with 10% FBS (Biological Industries) and 1% PenStrep (Corning). BEND3 (ATCC, CRL-2299, RRID:CVCL_0170) were cultured in Endothelial Cell Growth Medium MV2 (PromoCell) on 0.1% gelatin coated plastic. Primary human astrocytes (3H Biomedical) were cultured in Astrocyte Medium (3H Biomedical) and used below passage 15. U3082 glioma cells were obtained from HGCC (hgcc.se, RRID:CVCL_IR93) and were cultured in HGC medium on laminin-coated plates as described previously (18). Cells were acquired 2015 to 2020, tested quarterly for mycoplasma (Eurofins, MycoplasmaCheck), and not further authenticated.

Immunofluorescence

Cryosections were fixed in 4% PFA, followed by permeabilization in 0.3% Triton-x-100 and blocking in 1% BSA in PBS or DACO blocking reagent. Cryosections of organotypic slice cultures were fixed in 4% PFA followed by permeabilization in 0.1% Triton-x-100 and 0.1% sodium citrate then overnight incubation in 1% BSA or DAKO Diluent. Antibody combinations can be found in Supplemental Information. Images were acquired using an Olympus BX63 microscope and DP80 camera and cellSens Dimension v 1.12 software (Olympus; RRID: SCR_014551). Quantification was performed using ImageJ (RRID: SCR_003070) or Cell Profiler. All images were blinded for analysis.

Coculture

A total of 100,000 BEND3, HMC3, or PIGPC or 50,000 HBPV cells were pretreated with or without 10 Gy followed by 48 hours of coculture in DMEM with 100,000 PIGPC.

Irradiation

Irradiated pericytes, microglia, endothelial cells, and astrocytes were pretreated with 10 Gy in a CellRad x-ray irradiator (Faxitron).

Side population

SP was performed as described previously (19) with dual wavelength detection using 448/45 (Hoechst 33342-blue) and 613/18 (Hoechst 33342-red) filters.

Astrocyte-derived matrix

Confluent astrocytes were irradiated with 0 or 10 Gy followed by 10 days of culture on 0.2% gelatin in astrocyte medium supplemented with 50 μg/mL L-ascorbic acid (Sigma). After 10 days, plates were decellularized in 0.4 mmol/L NH_4OH (Fluka), 0.5% Triton X-100 in PBS with 1 mmol/L $CaCl_2$ and 0.5 mmol/L $MgCl_2$ (PBS-MC) at 37°C, washed with PBS-MC, then treated with 10 μg/mL DNAse I (Roche) for 1 hour at 37°C and stored in PBS-MC at 4°C.

Western blot analysis

Matrix lysates were prepared by scraping into 175 μL 4X Laemmli buffer (Bio-Rad;161–0747) containing 150 mmol/L DTT and boiling for 10 minutes. Whole cell lysates were prepared directly in 1:2 4X Laemmli buffer:RIPA with 50 mmol/L DTT. Blotting details can be found in Supplementary Information.

LC/MS-MS

Cell-derived matrix was solubilized for LC/MS-MS analysis according to Naba and colleagues (20). Detailed LC/MS-MS protocol can be found in Supplementary Information.

Phosphokinase array

The Proteome Profiler phosphokinase array (RND, ARY003C) was used according to manufacturer's instructions on U3082 grown for

Figure 1.

Irradiated astrocytes modify the extracellular matrix to promote stemness and radioresistance. **A,** Experimental design. **B–E,** SP of PIGPC after coculture with the indicated cell type pretreated with the indicated radiation dose. Dots represent individual experiments and bars represent average of all experiments with SEM. Sample FACS plots show gating for SP with insets showing FTC control gating. **B,** SP of PIGPC after coculture with either 0 Gy-treated PIGPC (0 Gy PIGPC), 0 Gy-treated BEND3 endothelial cells (0 Gy BEND3), 10 Gy-treated PIGPC cells (10 Gy PIGPC), or 10 Gy-treated BEND3 cells (10 Gy BEND3; $n = 7$). **C,** SP of PIGPC after coculture with either 0 Gy PIGPC, 0 Gy-treated HMC3 microglia (0 Gy HMC3), 10 Gy PIGPC, or 10 Gy-treated HMC3 cells (10 Gy HMC3; $n = 3$). **D,** SP of PIGPC after coculture with either 0 Gy PIGPC, 0 Gy-treated HVBP pericytes (0 Gy HVBP), 10 Gy PIGPC, or 10 Gy-treated HVBP cells (10 Gy HVBP; $n = 4$). **E,** SP of PIGPC after coculture with either 0 Gy PIGPC, 0 Gy-treated astrocytes (0 Gy Astro), 10 Gy PIGPC, or 10 Gy-treated astrocytes (10 Gy Astro; $n = 4$). *, $P \le 0.05$ by one-way ANOVA with Dunnet multiple comparison's posttest. **F,** Scatter plot showing percent SP of PIGPC cultured on ADMc or ADMi from $n = 3$ experiments and sample plots showing an example of gating for SP. Error bars, SEM. **, $P \le 0.01$, unpaired *t* test. **G,** Scatter plot showing SP of U3082 glioma cells cultured on ADMc or ADMi in serum-free conditions ($n = 4$) and sample plots showing an example of gating for SP. Error bars, SEM. **, $P \le 0.01$, ratio paired *t* test. **H,** Self-renewal of U3082 glioma cells preconditioned on ADMc or ADMi. Quantification of primary spheres (center) and secondary spheres (right; $n = 3$) with images of sample secondary spheres from the indicated preconditioning (left). Error bars, SEM. *, $P \le 0.05$, unpaired *t* test. **I,** Clonal survival of U251 glioma cells plated on ADMc or ADMi in triplicate wells, followed by irradiation with 0 or 4 Gy. Scatter plot indicates percent survival ($n = 3$ independent experiments). Example colonies are shown below. Error bars, SEM. *, $P \le 0.05$, unpaired *t* test. **J,** Sample of most altered gene sets in U3082 cells cultured on ADMi compared with ADMc. NES indicates change in the enrichment score of cells cultured on ADMi relative to ADMc.

Published OnlineFirst January 22, 2021; DOI: 10.1158/0008-5472.CAN-20-1785

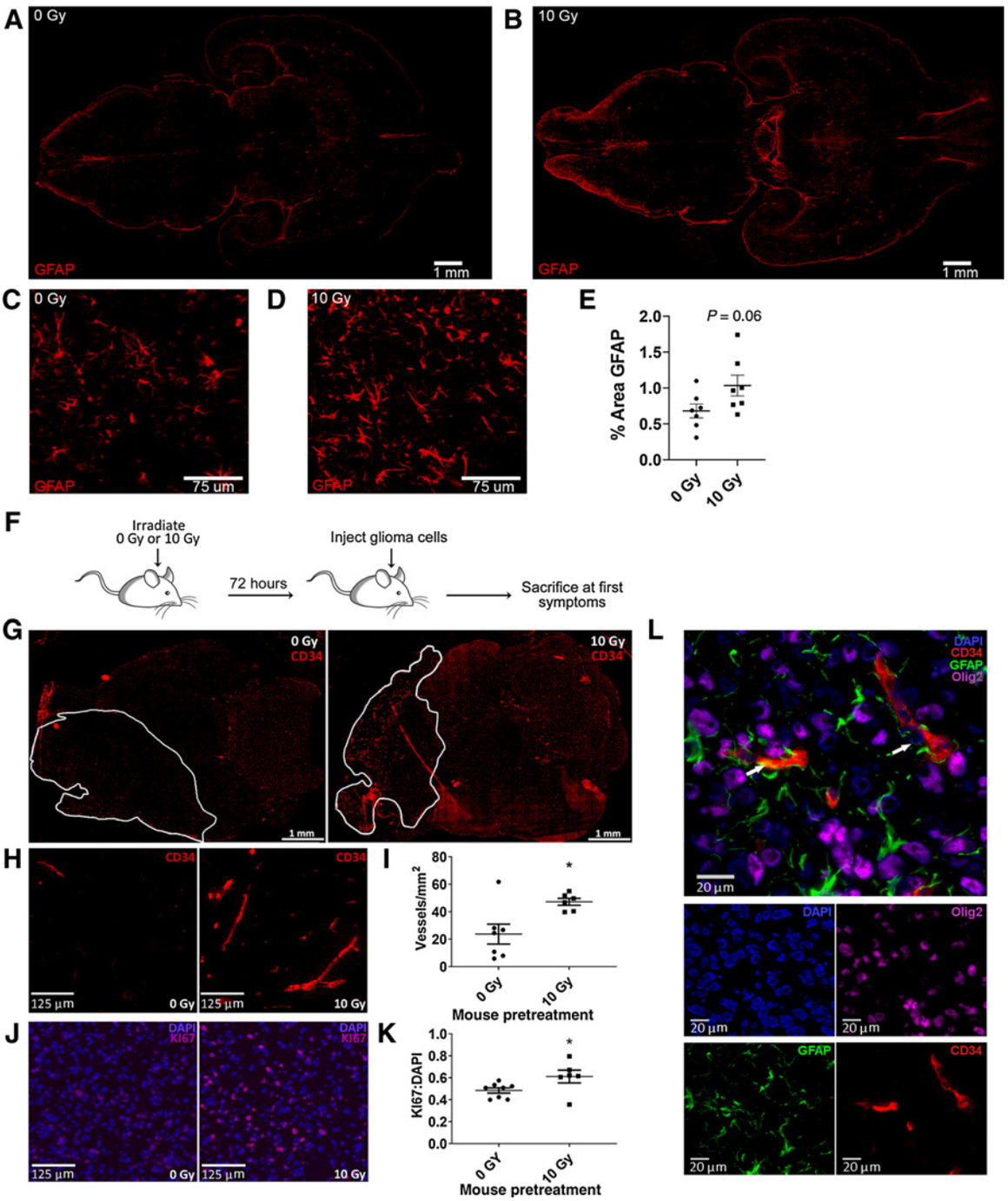

Figure 2.

The irradiated microenvironment supports tumor growth. **A** and **B,** Representative immunofluorescent detection of GFAP on whole brain scans of sections from non-tumor bearing mice treated with 0 Gy (**A**) or 10 Gy (**B**). **C** and **D,** High magnification image of GFAP-positive cells from **A** to **B**. **E,** Percent area GFAP staining in 0 and 10 Gy treated mice. Dots represent individual mice and bars average of all mice with SEM. *P* value, unpaired *t* test. **F,** Experimental design. **G,** Whole brain scans of sections from mice pretreated with the indicated dose of radiation prior to injection with glioma cells. Tumor-bearing brains stained for CD34 to identify vasculature. **H,** Examples of CD34 immunofluorescence marking microvascular proliferation in mouse gliomas from mice pretreated with the indicated dose of radiation. **I,** Quantification of microvascular proliferation in mice pretreated with 0 or 10 Gy. **J** and **K,** Examples of Ki67 (magenta) staining of tumors from mice pretreated with the indicated dose of radiation (**J**) and quantification of Ki67 relative to DAPI in those tumors (**K**). **I** and **K,** Dots represent results from individual mice. Bars represent average from $n = 8$ 0 Gy control mice and $n = 6$ 10 Gy irradiated mice. Error bars, SEM. *, $P \leq 0.05$, unpaired *t* test. **L,** Example of immunofluorescent staining of CD34 (red), glioma cells (Olig2; magenta), and the astrocyte marker GFAP (green). DAPI stains indicate nuclei (blue). White arrow, locations of association between astrocytes and vasculature.

Published OnlineFirst January 22, 2021; DOI: 10.1158/0008-5472.CAN-20-1785

24 hours on plates coated with either 0.1 μg/cm^2 laminin or laminin plus 3.3 mU/cm^2 TGM2.

ELISAs

Human ELISA kits for lysates for TNFα (Sigma; RAB1089), IL6 (Sigma; RAB0308), and IL8 (Sigma; RAB0319) were used according to manufacturer's instructions on lysates from astrocytes derived from 4 individual donors 24 hours after irradiation with 10 Gy. TNFα values were normalized to total protein in lysates. IL6 and IL8 were used as markers of astrocyte activation.

Colony assay

U251 cells were plated at 200 cells/well in a 6-well dish on ADMc or ADMi in DMEM. After 24 hours, dishes were irradiated with 0 or 4 Gy. Cells were cultured 2 weeks or until visible colonies formed. Colonies were fixed in 4% PFA, stained with 0.01% Crystal Violet for 1 hour, photographed on a LAS-3000 imaging system, then counted using Image J followed by visual confirmation.

Self-renewal

U3082 cells were cultured on ADMc or ADMi 5 days in HGC Media. For primary spheres, cells were dissociated with Accutase then replated in three wells each of 6-well dishes at 300 cells/mL in 2 mL HGC Media and cultured until visible spheres formed. Primary spheres were dissociated and replated as described above. Spheres were counted on a Zeiss AX10 inverted microscope.

Limiting dilution sphere-formation

U3082 cells were preconditioned on plates coated with either 0.1 μg/cm^2 laminin or laminin plus 3.3 mU/cm^2 TGM2 for 4 days followed by plating at a density of 300 cells/mL in 2 mL HGC media and culture until visible spheres formed. Primary spheres were dissociated then replated at 1,000 cells/mL in 300 μL in eight wells of a 48-well dish followed by serial 1:2 dilutions across eight columns in the presence or absence of 40 mU/mL TGM2 and the presence or absence of 10 nmol/L dasatinib until visible spheres formed. Any well containing a sphere was scored as positive. Limiting dilution assay was quantified using the analysis tool at http://bioinf.wehi.edu.au/software/elda/ (21).

RNA sequencing

Sequencing performed at the Center for Translational Genomics, Lund University and Clinical Genomics Lund, SciLifeLab, and National Genomics Infrastructure Stockholm Node, Science for Life Laboratory. Details in Supplementary Information.

Patient cohort analysis

The R2: Genomics Analysis and Visualization Platform (http://r2.amc.nl) was used to examine the Glioblasoma-The Cancer Genome Atlas (TCGA)-540 dataset (22). Astrocyte irradiation signature score was calculated using the *z*-score of the top 100 upregulated genes. Kaplan–Meier analysis using the scanning method was applied to the signature score using overall survival data and Bonferoni adjusted *P*-values of <0.05 were considered significant. Data from the Allen Institute for Brain Science IVY-GAP (http://glioblastoma.alleninstitute.org; RRID:SCR_005044) and the Chinese Glioma Genome Atlas (CGGA; ref. 23) were analyzed using the GlioVis data portal for visualization and analysis of brain tumor expression datasets (24, 25).

Organotypic slice culture

Freshly dissected brains were sliced into 300 μmol/L slices using a 5,100 mz vibrating blade tissue slicer (Campden Instruments). Slices were supported on polycarbonate tissue culture dish inserts with 0.4 μmol/L pore size for culture at 37°C, 5% CO_2 in HGC Medium. After overnight incubation, slices were treated with 0 or 5 μmol/L of the TGM2 inhibitor GK921 daily for 72 hours. Slices were PFA fixed then cryosectioned. Percent Olig2-positive nuclei were quantified using Cell Profiler (26).

Statistical analysis

All statistical analysis was performed in GraphPad Prism vs. 8.1.2 (RRID:SCR_002798). Statistical tests and number of replicates are indicated in figure legends. All *t* tests were two-tailed.

Patient glioma samples

Human biological samples were collected according to the Swedish guidelines for use of clinical material, which includes written informed consent from patients and approvals by the regional ethical committee (Dnr.2018/37). IDH mutation status was determined according to clinical routine.

Results

Irradiated astrocytes modify the extracellular matrix to promote stemness and radioresistance

We devised a coculture scheme to test control or irradiated stromal cells for their ability to increase one glioma stemness indicator, the side population (SP; ref. 19). Stromal cells were irradiated before coculturing with nonirradiated PDGFB-induced glioma primary cells (PIGPC) derived from RCAS-*PDGFB*-induced gliomas in *Nestin-tv-a Ink4a/Arf*$^{-/-}$ mice (PDG mice). Nonirradiated PIGPC were added to the pre-irradiated cells for coculture for 48 hours, followed by an SP assay (**Fig. 1A**).

We pretreated mouse brain endothelial cells (BEND3; **Fig. 1B**), human microglia (HMC3; **Fig. 1C**), primary human brain vascular pericytes (HBVP; **Fig. 1D**), and primary human astrocytes derived from individual donors (**Fig. 1E**) with 0 to 10 Gy radiation. PIGPC were used as controls. Only coculture with pre-irradiated astrocytes stimulated a consistent increase in SP of PIGPCs (**Fig. 1E**; Supplementary Figs. S1A and S1B), suggesting that irradiated astrocytes support glioma stemness. No SP was detected in stromal cells (Supplementary Figs. S1C and S1D). Coculture of PIGPC with irradiated PIGPC did not increase SP (**Fig. 1B–E**).

Coculture of astrocytes with glioma cells may increase the glioma cell SP through cell–cell contact, soluble factors, or modification of the extracellular matrix (ECM). We created conditioned media to test soluble factors by suspending astrocytes in sodium alginate beads followed by treatment with 0 to 10 Gy, then cocultured with PIGPC. No increase in SP of PIGPC cells cultured in conditioned media was detected (Supplementary Figs. S2A–S2C), suggesting the possibility of insoluble factors influencing the SP of PIGPCs.

To generate purified ECM, confluent astrocytes were treated with 0 to 10 Gy, cultured for 10 days, then de-cellularized, leaving behind insoluble matrix proteins (astrocyte derived matrix, ADM). Glioma cells were cultured on matrix from 10 Gy-irradiated astrocytes (ADMi) or nonirradiated astrocytes (ADMc) to examine the influence of ADM on SP, self-renewal, and survival after irradiation (Supplementary Fig. S2A).

PIGPC (**Fig. 1F**) and the serum-free cultured human glioma cell line U3082 (**Fig. 1G**) showed increased SP when cultured on ADMi, suggesting that changes in ADM proteins after irradiation increased the SP of glioma cells (**Fig. 1E**). No change was observed in mRNA of the stemness markers *NANOG, SOX2, OCT4*, and *ID1* after culture of

Published OnlineFirst January 22, 2021; DOI: 10.1158/0008-5472.CAN-20-1785

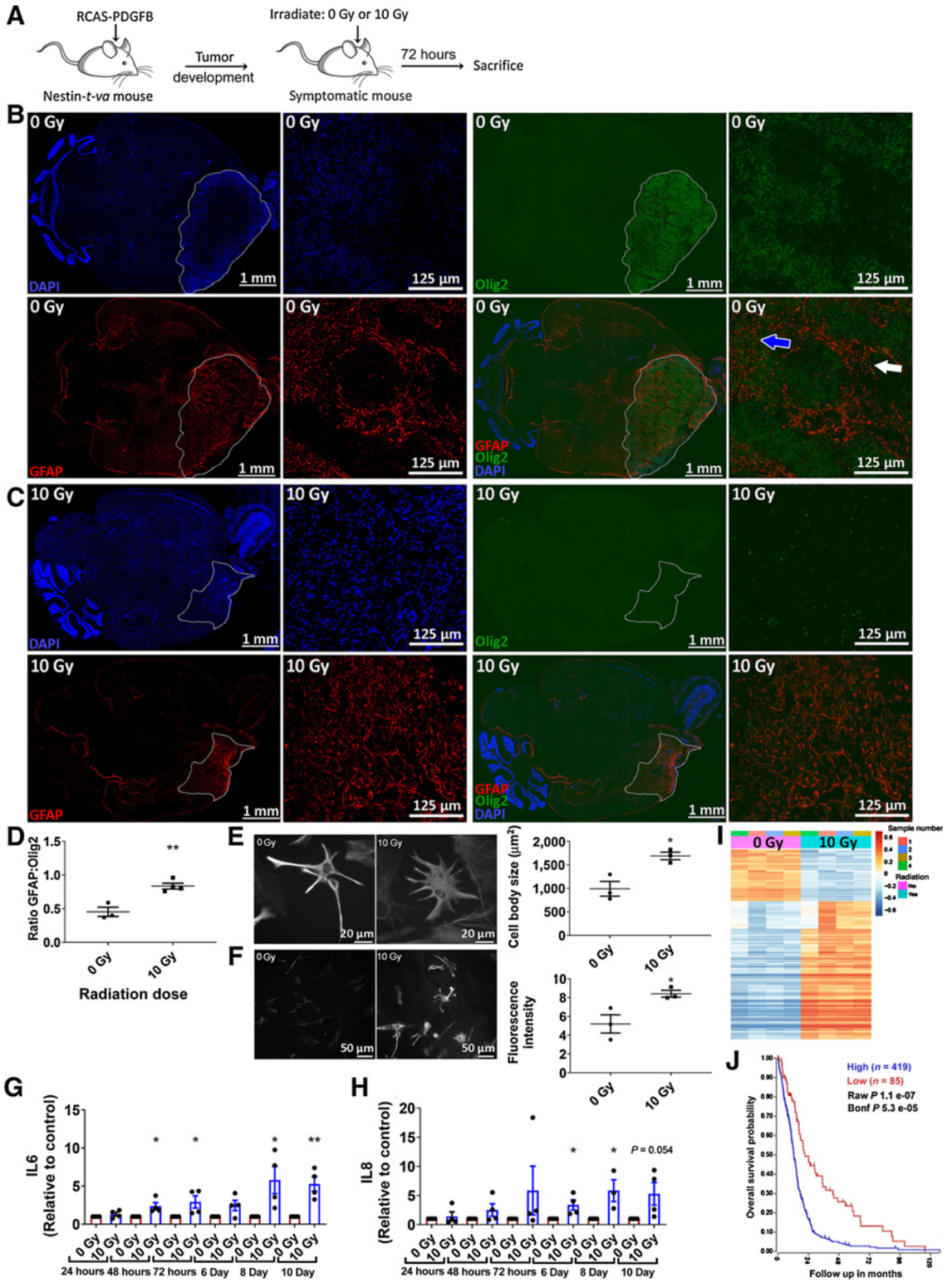

Published OnlineFirst January 22, 2021; DOI: 10.1158/0008-5472.CAN-20-1785

U3082 on ADMi (Supplementary Fig. S2D). We therefore looked at a functional assay measuring self-renewal by quantifying sphere-formation. U3082 cells were preconditioned for 5 days on ADMc or ADMi, then plated at clonal densities, followed by assessment of primary and secondary sphere formation. There were no changes in primary sphere numbers (**Fig. 1H**); however secondary spheres, the more accurate measure of self-renewal (27), increased from cells preconditioned on ADMi compared with ADMc (**Fig. 1H**). These data suggest that astrocytes modify the ECM after irradiation to support stemness.

To determine whether ADMi promotes radioresistance of glioma cells, we plated clonal densities of human glioma U251 cells on ADMc or ADMi, followed by irradiation at 4 Gy (**Fig. 1I**). Glioma cells cultured on ADMi showed increased colony formation after irradiation compared to cells cultured on ADMc (**Fig. 1I**), suggesting that matrix from irradiated astrocytes promotes radioresistance of glioma cells.

RNA sequencing of U3082 cells cultured on ADMc or ADMi for 48 hours revealed that culture on ADMi resulted in global gene expression changes of glioma cells. Among gene sets upregulated after culture on ADMi were pathways associated with the ECM, basement membrane, and integrin signaling (**Fig. 1J**); downregulated ones were associated with translation initiation and oxidative phosphorylation (**Fig. 1J**). No significant changes were recorded in individual stem cell marker genes including *SOX2, ID1, OCT4*, and *PROM1* (adjusted $P = 0.99$).

Together, these data suggest that astrocytes modify matrix proteins after irradiation in a manner promoting stemness, including radioresistance of glioma cells.

The irradiated microenvironment supports tumor growth

Finding that tumor-naïve astrocytes irradiated in culture can promote the SP of glioma cells, we sought to determine whether astrocytes in tumor-naïve brains show increased activation in response to irradiation. We stained brains from tumor-naïve mice treated with 0 to 10 Gy for GFAP, a marker of astrocyte activation, and identified a trend of increased GFAP in the brains of irradiated mice (**Fig. 2A–E**), consistent with previous findings at higher radiation doses (28).

We tested whether radiation-induced changes in the microenvironment influence tumor growth by pre-irradiating mice with 0 to 10 Gy to the brain, followed by intracranial injection with PIGPC 72 hours post-irradiation. Mice were sacrificed upon displaying glioma symptoms (**Fig. 2F**). Pre-irradiated mice developed tumors with increased microvascular proliferation (MVP; **Fig. 2G–I**) and increased Ki67-positive nuclei (**Fig. 2J** and **K**), indicators of more aggressive, high-grade glioma. Astrocytes were abundant within the tumor and associated with sites of MVP (**Fig. 2L**), one site enriched with stem-like glioma cells (11). These findings suggest that irradiation of the microenvironment supports tumor growth.

Reactive astrocytes persist within the tumor volume after irradiation

Astrocytes are an abundant cell type in the brain and in gliomas and are likely to survive radiotherapy (29). It is established that astrocytes respond to damage to the brain (30), including radiation (28) in a process termed reactive gliosis. Although this response varies, some hallmarks are commonly seen, including GFAP and vimentin upregulation and morphologic reorganization (30). Notably, tumors frequently recur in the astrogliotic regions overlapping with previous irradiation fields (3).

To understand the response of astrocytes to radiation, we examined purified human astrocytes *in vitro* and astrocytes from normal and tumor-bearing mouse brains *in vivo*. PDG mice were irradiated upon glioma symptoms with 0 to 10 Gy, then sacrificed 72 hours later (**Fig. 3A**). Whole brain sections were stained for Olig2, which marks glioma cells, and GFAP, which marks astrocytes (**Fig. 3B** and **C**). In 0 Gy-treated tumor-bearing brains, reactive astrocytes were enriched at the tumor borders and were found throughout the tumor, as seen in whole brain sections (**Fig. 3B**). Tumor area is demarcated with a line. Astrocytes were found within stromal compartments (white arrow in high-magnification, merged image) and among the Olig2-positive glioma cells (blue arrow; **Fig. 3B**).

After irradiation, Olig2-positive cells decreased to nearly undetectable levels; however, GFAP staining was retained in areas of the likely original tumor volume (**Fig. 3C**, white borders, identified by GFAP staining). This can be quantified by measuring the ratio of GFAP to Olig2 in the areas demarcated by strong GFAP staining (white borders; **Fig. 3D**), which revealed an increased ratio of GFAP to Olig2 in irradiated brains compared with control.

Because *in vitro* cultivation of primary astrocytes shifts them to a more reactive phenotype than seen *in vivo*, we tested whether primary cultured human astrocytes underwent features of reactive gliosis. Astrocytes exposed to 10 Gy developed the classic morphology of somatic hypertrophy (**Fig. 3E**) and expressed elevated levels of the reactive marker vimentin (**Fig. 3F**; ref. 30). Somatic hypertrophy and elevated vimentin could also be seen after three daily doses of 2 Gy (Supplementary Figs. S3A–S3C). Furthermore, irradiated astrocytes expressed increased levels of the soluble proteins IL6 (**Fig. 3G**) and IL8 (**Fig. 3H**), which remained for up to 10 days, indicating a persistent radiation response.

To characterize the astrocytic response to radiation in culture, we performed RNA sequencing on purified human astrocytes 24 hours after a dose of 0 to 10 Gy *in vitro*. Irradiated astrocytes had a distinct gene expression pattern from control astrocytes (**Fig. 3I**), including upregulation of *GFAP* ($P = 4.6E{-}16$). Gene set enrichment data revealed an atypical response to irradiation compared with other cell types, such as suppression of the p53 pathway, which has been seen previously in astrocytes (31), as well as elevation of gene sets involved in DNA repair and cell cycle (Supplementary Table S1).

Figure 3.

Reactive astrocytes persist within the tumor volume after irradiation. **A,** Experimental design. **B** and **C,** Sections of brains from Nestin-*tv-a* mice injected with RCAS-*PDGFB* and treated upon symptoms with 0 Gy (**B**) or 10 Gy (**C**). Immunofluorescent detection of astrocytes with GFAP (red) and tumor with Olig2 (green) in whole brain scans and high magnification details from the tumor region of mouse brain sections. Nuclei are stained with DAPI (blue). White outline in **B** indicates Olig2-positive tumor area. White line in **C** indicates probable tumor location before irradiation based on site of injection and GFAP-positivity. **D,** Quantification of GFAP relative to Olig2 measured in **B** (0 Gy) within Olig2-positive tumor area or (10 Gy) within area of retained GFAP positivity (**C**). White line in **C** indicates example of boundary where GFAP:Olig2 ratio was measured. Scatter plot of $n = 3$ mice from each treatment. *, $P \le 0.05$, unpaired *t* test. **E,** Immunofluorescent detection of GFAP in cultured astrocytes 24 hours after 0 or 10 Gy and quantification of astrocyte body size ($n = 3$). *, $P \le 0.05$, unpaired *t* test. **F,** Immunofluorescent detection of vimentin in cultured astrocytes 24 hours after 0 or 10 Gy and quantification of fluorescence intensity normalized to number of nuclei in image ($n = 3$). *, $P \le 0.05$, ratio paired *t* test. **G** and **H,** Quantification by ELISA of IL6 (**G**) and IL8 (**H**) in conditioned medium from astrocytes, indicated time after treatment with 0 or 10 Gy ($n = 3$). *, $P \le 0.05$; **, $P \le 0.01$, unpaired *t* test. ELISA results were normalized to total protein. Scatter plots represent values relative to the respective time point control. **I,** Heatmap of RNA sequencing results of astrocytes 24 hours after 0 or 10 Gy. **J,** Kaplan–Meier curve showing survival of glioma patients with high (blue) or low (red) expression of genes expressed by irradiated astrocytes. All error bars are SEM.

Published OnlineFirst January 22, 2021; DOI: 10.1158/0008-5472.CAN-20-1785

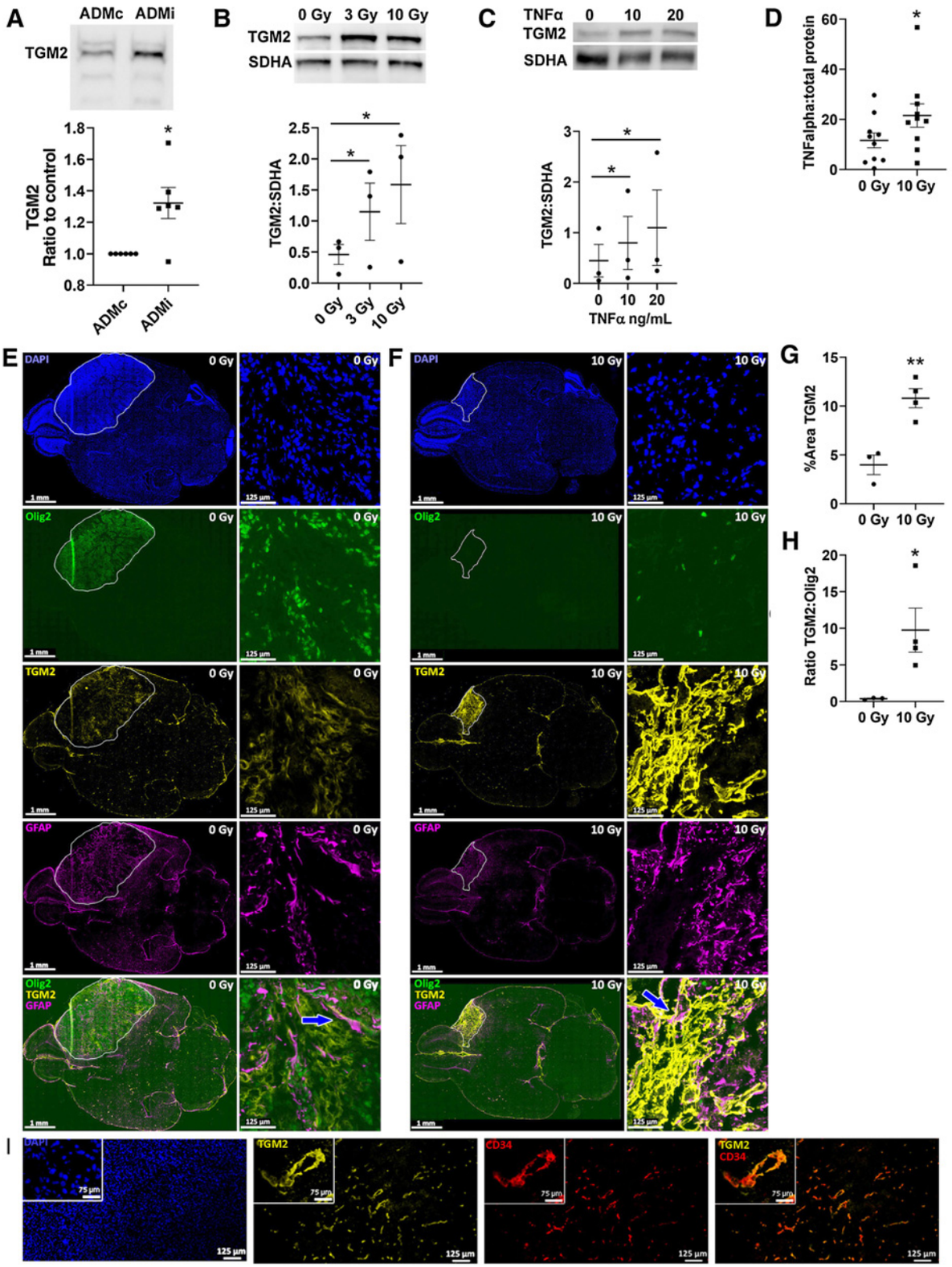

Published OnlineFirst January 22, 2021; DOI: 10.1158/0008-5472.CAN-20-1785

A gene signature consisting of the 100 most upregulated genes in irradiated astrocytes as compared with controls was significantly associated with worse survival in GBM, based on analysis of TCGA GBM dataset (**Fig. 3J**; ref. 22).

Irradiated astrocytes secrete TGM2 after irradiation

To identify proteins in the ECM responsible for increased radioresistance of cells cultured on ADMi, we performed mass LC/MS-MS analysis on ADMc and ADMi. Supplementary Table S2 lists proteins in the matrix that showed the greatest changes. Among the potential targets identified within this altered ECM, we selected TGM2 for further inquiry because of its proposed roles in matrix modification and stemness (32, 33), as well as promising results in a previous glioma xenograft model (33, 34) and reports that it is a prognostic indicator of shorter time to relapse after chemoradiotherapy (35).

We first confirmed by Western blot increased expression of TGM2 in matrix from astrocytes from different donors (**Fig. 4A**). We also confirmed increased TGM2 in total cell lysates from astrocytes after stimulation with 3 or 10 Gy (**Fig. 4B**). Previous studies have shown that TGM2 in glioma cells is upregulated in response to TNFα stimulation (34). In primary human astrocytes, stimulation with TNFα increased expression of TGM2 (**Fig. 4C**) and TNFα was elevated after irradiation (**Fig. 4D**), suggesting that TGM2 increase after irradiation may be dependent on TNFα.

We followed this by examining TGM2 expression *in vivo* in PDG mice (**Fig. 3A**). Whole brain sections were stained for Olig2, TGM2, and GFAP (**Fig. 4E** and **F**). Relative to nontumor bearing brain tissue, TGM2 expression was elevated in tumors (white bounded area, **Fig. 4E**), was extensively expressed in the stromal compartment, and showed areas of co-staining with GFAP (**Fig. 4E**, example: blue arrow, merged high magnification image). In the tumors treated with 10 Gy (**Fig. 4F**), TGM2 expression was retained in the likely original tumor volume and even increased, resulting in a greater percent area covered by TGM2 (**Fig. 4G**). Within the area of TGM2-positive staining, quantification of TGM2 relative to Olig2 (**Fig. 4H**) indicates that TGM2 remains even after the Olig2-positive tumor cells have been depleted by irradiation. In the irradiated tumors, regions of TGM2 staining were also found in close association with GFAP-positive astrocytes, often co-staining or showing astrocytes surrounding areas of intense TGM2-positivity (**Fig. 4F**, example: blue arrow, merged high magnification image).

Like GFAP, TGM2 expression is elevated in areas of MVP and the normal vasculature (**Fig. 4I**). Comparable to our findings in mice, analysis of the Ivy Glioblastoma Atlas Project (IVY-GAP; ref. 24) reveals that *TGM2* is highly elevated in areas of MVP (Supplementary Fig. S4).

Taken together, these data suggest that irradiation promotes increased expression of TGM2 from astrocytes, potentially providing a radio-protective environment for a newly expanding tumor. We therefore returned to our *in vitro* experimental systems to determine if there was a functional relationship between TGM2 and stemness and radiation resistance of glioma cells.

Astrocyte-derived TGM2 promotes glioma stemness after irradiation

To determine whether TGM2 expression might be associated with glioma cell stemness or radiation resistance, we examined the effects of either purified TGM2 or TGM2 inhibitors on our *in vitro* model of glioma cell–astrocyte matrix interaction. Purified TGM2, when coated onto ADMc, raised the SP of PIGPC near to that seen with PIGPC cultured on ADMi (**Fig. 5A**). In contrast, two different TGM2 inhibitors, GK921 (**Fig. 5B**) and dansylcadaverine (DC; **Fig. 5B**), decreased the SP of PIGPC cultured on ADMi to the levels seen on ADMc. GK921 also decreased survival after irradiation of PIGPC cultured on ADMi to levels seen on ADMc, while not affecting PIGPC cultured on ADMc (**Fig. 5C**; Supplementary Fig. S5). These data suggest that extracellular TGM2 contributes to the increased stemness and radiation resistance of glioma cells cultured on ADMi as compared with those cultured on ADMc.

In vivo, tumors treated with 10 Gy increased CD44 expression (**Fig. 5D–G**), a stem cell marker in glioma (36) and a marker of mesenchymal subtype GBM. CD44 strongly colocalized with TGM2 (**Fig. 5F** and **G**). Like TGM2, CD44 expression was retained in the likely original tumor volume after irradiation, even as the Olig2-positive cells receded, as seen by increased expression relative to Olig2 (**Fig. 5G**). These data provide evidence that TGM2 is associated with increased stemness *in vivo* and is elevated after irradiation.

TGM2 increases signaling through the integrin-β1/Src pathway

We next sought to determine which TGM2-stimulated signaling pathways may promote stemness in glioma cells. We performed a phosphokinase array to screen for potential changes in signaling in U3082 cells cultured on plates coated with 3.3 mU/cm^2 TGM2 (**Fig. 6A** and **B**; Supplementary Table S3). Among the most highly increased phosphorylation events, proteins involved in the integrin-β1 pathway were increased, including GSK3β, Fgr, β-catenin, EGFR, JNK1/2/3, and Src (37). GSEA of U3082 cultured on ADMc and ADMi indicated a trend toward enrichment of the Integrin1 pathway in cells cultured on ADMi (**Fig. 6C**). In addition, integrin-β1 is linked to fibronectin signaling, which is directly affected by TGM2 (38). We therefore examined expression of integrin-β1 in tumors from PDG mice 72 hours post-irradiation. Integrin-β1 expression was closely associated with

Figure 4.

Irradiated astrocytes secrete TGM2 after irradiation. **A,** Representative Western blot analysis of TGM2 in ADMc and ADMi. Quantification from $n = 6$ independent samples of ADMc and ADMi. Error bars, SEM. *, $P \le 0.05$ by ratio paired *t* test. **B,** Representative Western blot analysis of TGM2 from total cell lysates of astrocytes collected 96 hours after irradiation with 0, 3, or 10 Gy. Quantification of $n = 3$ independent samples normalized to SDHA loading control. Error bars, SEM. *, $P \le 0.05$ ratio paired *t* test. **C,** Representative Western blots of TGM2 in astrocytes 96 hours after stimulation with 0, 10, or 20 ng/mL TNFα. Quantification of $n = 3$ independent samples normalized to SDHA loading control. Error bars, SEM. *, $P \le 0.05$, ratio paired *t* test. **D,** Quantification of human TNFα normalized to total protein in lysates from $n = 10$ independent experiments. *, $P \le 0.05$ ratio, paired *t* test. **E–G,** Sections of brains from PDG mice treated upon symptoms with either 0 Gy (**E**) or 10 Gy (**F**). Immunofluorescent detection with Olig2 (green, tumor), TGM2 (yellow), and GFAP (magenta, astrocytes) in whole brain scans and high magnification details of mouse brain sections are presented. Nuclei are stained with DAPI (blue). White outline in **E** indicates Olig2-positive tumor area. White line in **F** indicates probable tumor location before irradiation based on site of injection and TGM2-positivity. **G,** Quantification of percent area covered by TGM2 within the nonirradiated Olig2-positive tumor area (white outline in **E** or within the area of retained TGM2 positivity in the irradiated tumors). White line in **F** indicates example of boundary where TGM2 was measured. Scatter plot represents $n = 3$ mice from each treatment. Error bars, SEM. *, $P \le 0.05$, unpaired *t* test. **H,** Quantification of TGM2 relative to Olig2 measured in **E** (0 Gy) within Olig2-positive tumor area or **D** (10 Gy) within area of retained TGM2 positivity. White line in **F** indicates example of boundary where TGM2 to Olig2 ratio was measured. Scatter plot represents $n = 3$ mice from 0 Gy and $n = 4$ mice from 10 Gy treatment. Error bars, SEM. *, $P \le 0.05$, unpaired *t* test. **I,** Example of CD34-labeled blood vessels (red) co-stained with TGM2 (yellow) with high magnification inset.

Published OnlineFirst January 22, 2021; DOI: 10.1158/0008-5472.CAN-20-1785

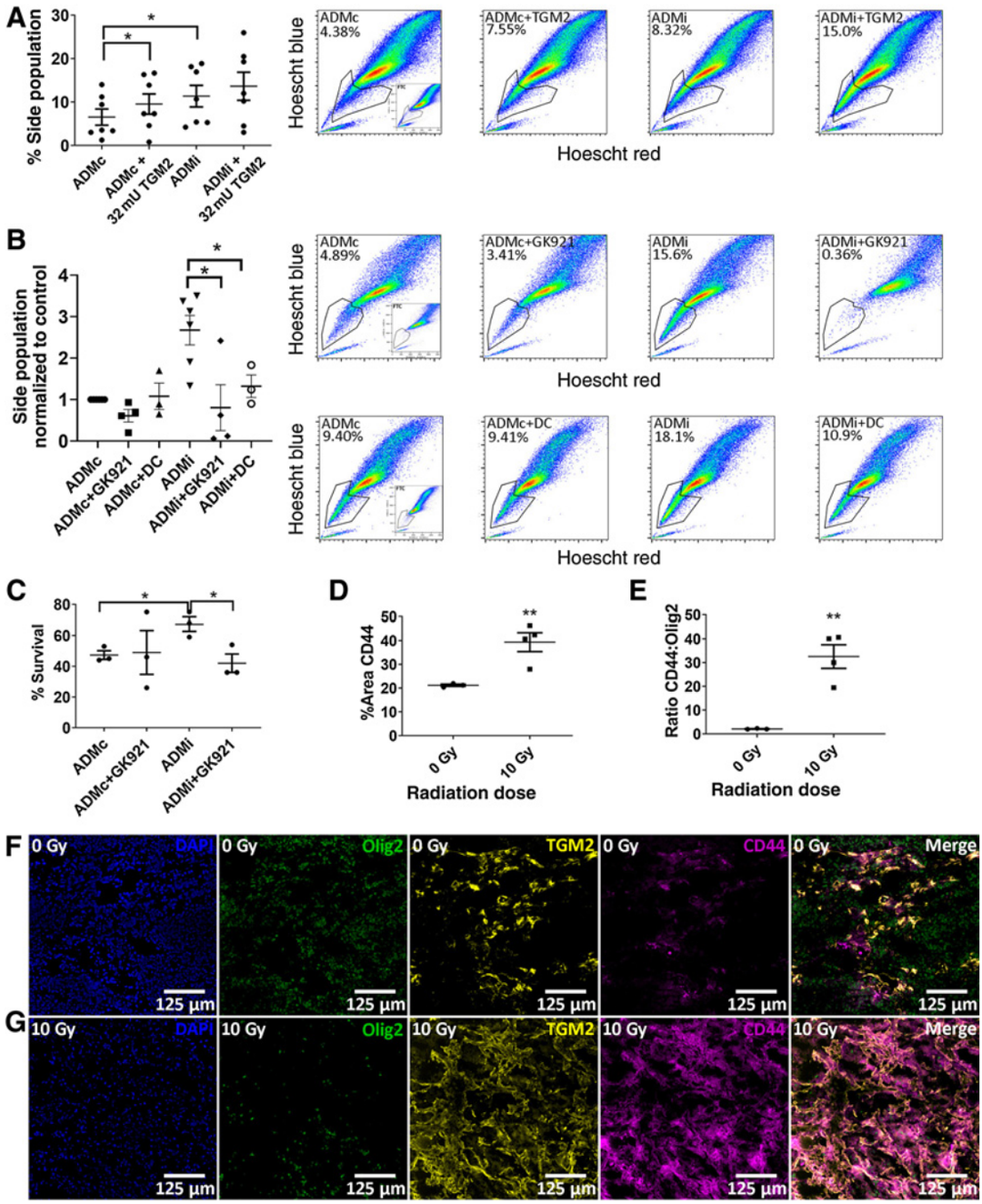

Figure 5.

Astrocyte-derived TGM2 promotes glioma stemness after irradiation. **A,** Quantification of $n = 7$ independent assays in which PIGPC glioma cells were cultured on ADMc or ADMi coated with vehicle or 32 mU TGM2 (left). Sample FACS plots with gating (right). *, $P \le 0.05$, one-way ANOVA with Dunnet multiple comparison's posttest. **B,** Quantification of PIGPC cultured on ADMc or ADMi with 0.5 µmol/L of the TGM2 inhibitor GK921 ($n = 4$) or 100 µmol/L of the TGM2 inhibitor dansylcadaverine (DC; $n = 3$). Values are normalized to the ADMc control. Error bars, SEM. *, $P \le 0.05$, unpaired t test. Right, sample FACs plots with gating. **C,** Clonal survival of U251 glioma cells plated on ADMc or ADMi in triplicate wells in media containing 0.1 µmol/L GK921, followed by irradiation with 0 or 4 Gy. Scatter plot indicates average percent survival ($n = 3$; left). Error bars, SEM. *, $P \le 0.05$, unpaired t test. **D,** Quantification of percent area covered by CD44 within the nonirradiated Olig2-positive tumor area or within the area of retained CD44 positivity in the irradiated tumors. (Boundaries indicated in **Fig. 4E** and **F** by white line.) Scatter plot represents $n = 3$ mice from 0 Gy and $n = 4$ mice from 10 Gy treatment. Error bars, SEM. **, $P \le 0.01$, unpaired t test. **E,** Quantification of CD44 relative to Olig2 measured within Olig2-positive tumor area in 0 Gy-treated mice or within area of retained TGM2 positivity in 10 Gy-treated mice. (Boundaries indicated in **Fig. 4E** and **F** by white line.) Scatter plot represents $n = 3$ mice from 0 Gy and $n = 4$ mice from 10 Gy treatment. Error bars, SEM. *, $P \le 0.05$, unpaired t test. **F** and **G,** Representative image of immunofluorescent detection of CD44 (magenta), TGM2 (yellow), and Olig2 (green) with co-staining of CD44 with TGM2 (white) within the tumor area in mice treated with either 0 Gy (**F**) or 10 Gy (**G**).

Published OnlineFirst January 22, 2021; DOI: 10.1158/0008-5472.CAN-20-1785

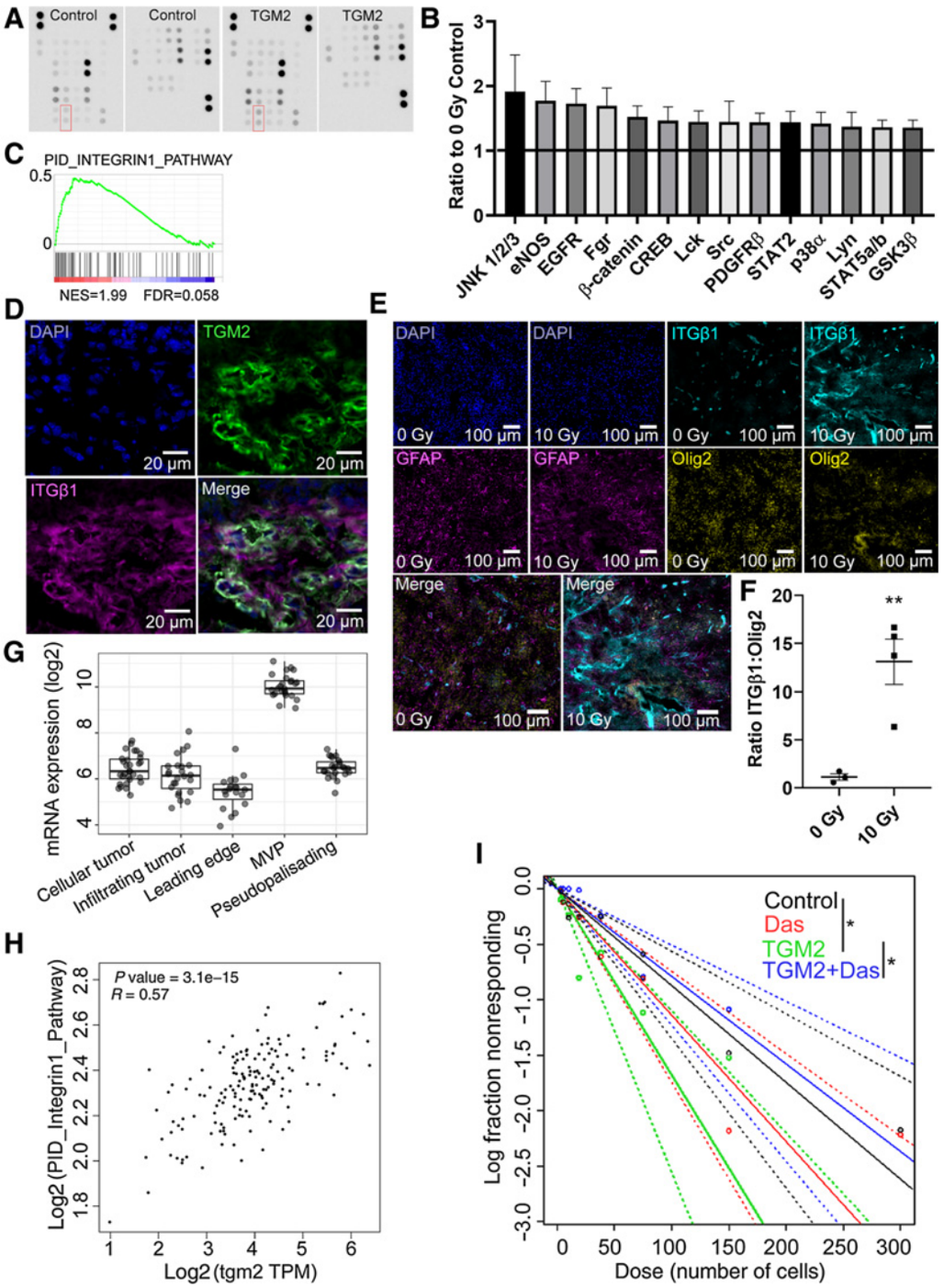

Figure 6.

TGM2 increases signaling through the integrin-β1/Src pathway. **A,** Representative blots of phosphokinase array of U3082 cells plated with or without TGM2. Src immunodetection indicated with red box. **B,** Quantification from $n = 3$ phosphokinase arrays. Bars represent average change of TGM2 relative to control in samples with an average change above 1.4. Errors bars, SEM. **C,** GSEA of PID_INTEGRIN1_PATHWAY. **D,** Representative immunodetection of TGM2 (green), integrin-β1 (magenta), and merge (white) association in PDG mouse tumors. DAPI, blue. **E,** Representative immunodetection of GFAP (magenta), Olig2 (yellow), integrin-β1 (cyan), and merge (white) 72 hours after treatment with 0 or 10 Gy. **F,** Quantification of ratio of integrinβ1 relative to Olig2 in PDG mice in tumor area (0 Gy; $n = 3$) or previous tumor area (10 Gy; $n = 4$). Dots represent data points from individual mice. Line, mean. Error bars, SEM. **, $P \leq 0.01$, unpaired t test. **G,** TGM2 transcript expression in the indicated histologic region of gliomas. MVP, microvascular proliferation. **H,** Correlation between TGM2 expression and expression of the PID_INTEGRIN1_PATHWAY in the TCGA GBM dataset. **I,** Representative log-fraction plot of the limiting dilution sphere formation assay. The slope of the solid line is the log-active cell fraction, with the dotted line showing the 95% confidence interval of the indicated treatments on U3082 glioma cells. *, χ^2, $P \leq 0.05$.

Published OnlineFirst January 22, 2021; DOI: 10.1158/0008-5472.CAN-20-1785

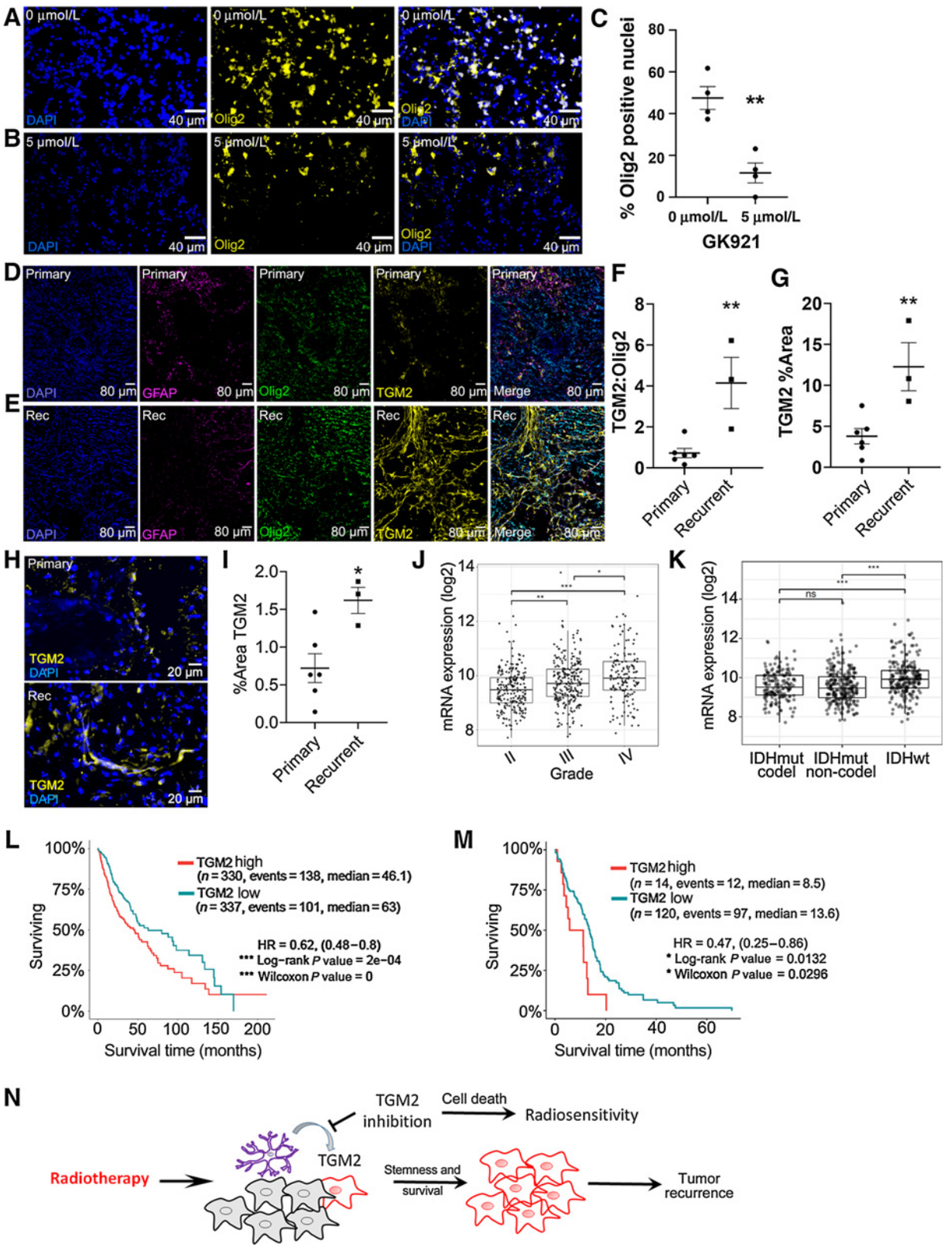

Published OnlineFirst January 22, 2021; DOI: 10.1158/0008-5472.CAN-20-1785

and frequently costained with TGM2 in tumors (**Fig. 6D**). Like TGM2, integrin-β1 remained in the original tumor volume after irradiation even after Olig2-positive cells were depleted, as can be seen when measured as ratio of integrin-β1 to Olig2 (**Fig. 6E** and **F**). According to the IVY-GAP database, like TGM2, integrin-β1 is associated with MVP (**Fig. 6G**). Furthermore, there is a significant correlation between TGM2 expression and the PID_INTEGRIN1_ PATHWAY in the TCGA GBM dataset (**Fig. 6H**) when analyzed in the Gene Expression Profiling Interactive Analysis (GEPIA2) web server (39).

To determine whether there was a functional relationship between the integrin-β1 pathway and the ability of TGM2 to promote stemness features of glioma cells, we examined whether inhibition of Src family kinases with dasatinib could block the stemness promoting properties of TGM2. We performed a limiting dilution self-renewal assay on U3082 preconditioned on either 0 or 3.3 mU/cm^2 TGM2 for 4 days. Preconditioned U3082 were allowed to form primary spheres in the presence or absence of 40 mU/ml TGM2, then dissociated spheres were replated in a limiting dilution assay in the presence or absence of TGM2 and 10 nmol/L dasatinib. TGM2 increased sphere-forming potential of U3082 relative to control cells while dasatinib decreased sphere formation in TGM2-treated cells but not in control cells (**Fig. 6I**; Supplementary Table S4). Taken together, these data suggest that stemness is promoted by TGM2 through a Src-related pathway as part of enhanced integrin-β1 signaling.

TGM2 is a potential therapeutic target in GBM

To further examine the effects of TGM2 inhibition, we used an *ex vivo* organotypic slice model of GBM. We initiated tumors in PDG mice by injection with RCAS-*PDGFB* and shp53, then sliced freshly-harvested brains upon detection of glioma symptoms. Slices were cultured overnight, followed by treatment with 0 or 5 μmol/L of the TGM2 inhibitor GK921 for 72 hours, then fixed and cryosectioned, followed by immunofluorescent detection of Olig2 to determine the presence of tumor cells. TGM2 inhibitor significantly decreased the percent of Olig2-positive nuclei in the sections, in some cases reducing Olig2-positive cells to undetectable levels (**Fig. 7A–C**).

To examine TGM2 expression in a model of recurrent glioma, we initiated tumors in PDG mice with RCAS-*PDGFB* and sh*Pten*. Mice were treated at symptoms with either 0 Gy or a fractionated dose of 2 Gy daily for 5 days, then sacrificed upon recurrence of glioma symptoms. Immunodetection of TGM2 and Olig2 revealed that elevated TGM2 is retained in the tumor recurrence (**Fig. 7D–G**), showing increases both relative to Olig2 (**Fig. 7F**) as well as in percent area covered in the tumor (**Fig. 7G**) as compared to the untreated primary tumors.

A small sample of human isocitrate dehydrogenase wild type (IDHwt) GBM showed elevated TGM2 protein expression in recurrent versus primary GBM (**Fig. 7H** and **I**). Recurrent tumors were from patients receiving radiotherapy of 60 Gy and temozolomide adjuvant therapy. While the sample size is small, this finding, in combination with the results from our mouse model, suggests higher TGM2 has the potential to remain in the GBM microenvironment at recurrence. This is further supported by an analysis of recurrent tumors in the TCGA and CGGA database, which both show a small but significant increase in *TGM2* mRNA in recurrent tumors compared to primary tumors (Supplementary Figs. S6A and S6B).

In primary human glioma, *TGM2* mRNA is elevated as tumor grade increases (**Fig. 7J**). *TGM2* mRNA is significantly increased in IDHwt tumors (**Fig. 7K**), the most aggressive tumor classification. Elevated *TGM2* correlates with shorter survival times (**Fig. 7L**). Although these shorter survival times are possibly the result of the association of elevated *TGM2* with increasing grade, it is notable that within IDHwt GBM, tumors with the top 10% of *TGM2* mRNA expression have the shortest survival times (**Fig. 7M**). Taken together, these data suggest that TGM2 may be a viable target in GBM.

On the basis of our findings, we propose a model in which radiation stimulates tumor-associated astrocytes to secrete TGM2, which then promotes stemness and survival of glioma cells, allowing tumor recurrence (**Fig. 7N**).

Discussion

GBM treatment options are limited after tumor recurrence. As surgery can rarely eliminate all GBM cells, identifying and targeting pathways that support GBM cell survival after radiotherapy is essential to improving outcomes. To this end, a better understanding of the effects of radiation on all aspects of a tumor's biology is needed. Studies so far have identified that radiation can promote the migration and invasion of tumor cells (40, 41), particularly by stimulating inflammation in the tumor microenvironment, such as that mediated by IL1β in a pre-irradiation model of glioma in rat brains (41, 42). Although some studies have examined how the tumor microenvironment can promote radiation resistance and GBM stemness (10, 43–45), little study has been made of how the stromal cells themselves respond to treatment modalities to support these features (46). This is an important question, as findings presented here suggest that stromal cells may respond to radiation in ways that could prime the microenvironment for protection of GBM cells against further radiation insults.

Figure 7.

TGM2 is a potential therapeutic target in GBM. **A** and **B,** Immunofluorescent detection of Olig2 (yellow) or nuclei (DAPI, blue) in cryosections of organotypic brain slices from mice bearing gliomas. Brain slices were treated with either 0 μmol/L (**A**) or 5 μmol/L (**B**) of the TGM2 inhibitor GK921. **C,** Quantification of percent of nuclei positive for Olig2 in organotypic brain slices from four mice. **D–G,** Mice were euthanized upon glioma symptoms to generate primary tumors or treated with 2 Gy daily for 5 days and euthanized upon tumor recurrence. **D** and **E,** Immunofluorescent detection of GFAP (magenta), Olig2 (green), TGM2 (yellow), and DAPI (blue) with representative images from primary tumors (**D**) or recurrent tumors (Rec; **E**). **F,** Quantification of ratio of TGM2 relative to Olig2 in $n = 6$ primary or $n = 3$ recurrent tumors. Dots represent data points from individual mice. Line, mean. Error bars, SEM. **, $P \le 0.01$, unpaired *t* test. **G,** Quantification of ratio of percent area covered by TGM2 in $n = 6$ primary or $n = 3$ recurrent tumors. Dots represent data points from individual mice. Line, mean. Error bars, SEM. **, $P \le 0.01$, unpaired *t* test. **H,** Representative images from primary or recurrent human glioma showing DAPI (blue) or TGM2 (yellow). **I,** Scatter plot showing elevated TGM2 in recurrent human glioma. Each point represents the average percent area of TGM2 from six areas measured within a tumor section from one of six patients (primary) or one of three patients (recurrent). *, $P \le 0.05$, unpaired *t* test. **J,** TGM2 transcript expression in glioma grades II, III, and IV. **K,** TGM2 transcript expression in IDH mutant (IDHmut) glioma with or without 1p/19q codeletion (codel and non-codel, respectively) or IDHwt glioma. **L,** Kaplan–Meier curve showing survival of glioma patients with either high (red) or low (blue) TGM2 expression. **M,** Kaplan–Meier curve showing survival of GBM patients with IDHwt tumors with TGM2 transcript expression in the upper 10% (red) or lower 90% (blue). **N,** Proposed model of stimulation of TGM2 release from astrocytes after irradiation and its role in survival of tumor cells. Grey cells, glioma cells that respond to radiotherapy. Red cells, glioma cells that survive radiotherapy. Purple cells, astrocytes.

Published OnlineFirst January 22, 2021; DOI: 10.1158/0008-5472.CAN-20-1785

It is likely that effects of radiotherapy on the tumor microenvironment are not limited to its effect on astrocytes described here. Although our coculture screen of pre-irradiated stromal cells detected a SP increase only from pre-irradiated astrocytes, our screen may favor our ability to detect the effect of irradiated astrocytes on glioma cells over other cell types. The use of the SP assay as a readout and the combination of human stromal cells with mouse glioma cells may have limited our findings. Other model systems may reveal further important interactions. However, despite astrocytes being derived from multiple different human donors, which reflects the variability seen in human populations in the TCGA and IVY-GAP datasets, we were still able to detect radiation-driven pathways that resulted in identification of a potential target for glioma therapy.

This study provides a promising new strategy in GBM treatment by examining lasting changes to the tumor microenvironment made by stromal cells in response to radiotherapy, changes that may support radiation resistance of GBM cells. Although previous work has shown that in untreated tumors, astrocytes react to the GBM microenvironment and can promote glioma growth (14), we have identified astrocytes as persisting within the original tumor volume even after the tumor bulk is killed by radiation, altering that environment in a radioprotective manner. We demonstrate that they do this by secreting TGM2, which supports stemness and radioresistance of GBM cells. This is an important addition to studies examining TGM2 expression in glioma cells themselves, and may shed light on previous findings that the TGM2 promoter is hypermethylated in glioma, yet TGM2 expression in GBM is elevated (47). Understanding the role of astrocytes in radiation response and TGM2 release may also further elucidate previous findings that TGM2 inhibition increased survival in a glioma xenograft model (33, 34).

Although we identified an important role for the integrin-β1 and Src pathways in TGM2 mediation of radiation resistance and stemness of glioma cells, the mechanisms by which TGM2 protects GBM should be further explored. Fibronectin bundling, perhaps the most well-described function of TGM2 (38), influences radiation resistance (48), angiogensis (49), and invasiveness, and integrin-β1 signaling (50), suggesting further study of fibronectin bundling and other matrix alterations post-irradiation is warranted. Our findings suggest a new strategy for sensitizing GBM cells to radiotherapy by short-circuiting the normal brain's protective response to radiation.

Authors' Disclosures

A. Pietras reports grants from Ragnar Söderberg Foundation, The Swedish Cancer Society, The Swedish Research Council, The Swedish Childhood Cancer Fund, Ollie & Elof Ericssons Foundation, Jeanssons Stiftelser, The Crafoord Foundation, Gösta Miltons Donationsfond, and Stiftelsen Cancera during the conduct of the study. No disclosures were reported by the other authors.

Authors' Contributions

T.J. Berg: Conceptualization, data curation, formal analysis, investigation, methodology, writing–original draft, writing–review and editing. **C. Marques:** Formal analysis, investigation, writing–review and editing. **V. Pantazopoulou:** Formal analysis, investigation, writing–review and editing. **E. Johansson:** Formal analysis, investigation, writing–review and editing. **K. von Stedingk:** Formal analysis, investigation, writing–review and editing. **D. Lindgren:** Formal analysis, investigation, writing–review and editing. **P. Jeannot:** Formal analysis, investigation, writing–review and editing. **E.J. Pietras:** Formal analysis, investigation, writing–review and editing. **T. Bergström:** Formal analysis, investigation, writing–review and editing. **F.J. Swartling:** Formal analysis, investigation, writing–review and editing. **V. Governa:** Investigation, writing–review and editing. **J. Bengzon:** Formal analysis, investigation, writing–review and editing. **M. Belting:** Formal analysis, supervision, investigation, writing–review and editing. **H. Axelson:** Formal analysis, supervision, investigation, writing–review and editing. **M. Squatrito:** Conceptualization, resources, data curation, formal analysis, supervision, funding acquisition, investigation, methodology, writing–original draft, project administration, writing–review and editing. **A. Pietras:** Conceptualization, resources, data curation, formal analysis, supervision, funding acquisition, investigation, methodology, writing–original draft, project administration, writing–review and editing.

Acknowledgments

The authors thank Christina Möller for technical assistance. The authors acknowledge support from Science for Life Laboratory, the National Genomics Infrastructure, NGI, and Uppmax for providing assistance in massive parallel sequencing and computational infrastructure. They acknowledge the Center for Translational Genomics, Lund University and Clinical Genomics Lund, SciLifeLab Sequencing for sequencing performed in their labs. They acknowledge the Preclinical Cancer Treatment Center, SciLifeLab, Uppsala University, for technical assistance and support with radiation therapies experiments *in vivo*. Support from the Swedish National Infrastructure for Biological Mass Spectrometry is gratefully acknowledged. The results shown here are in whole or part based upon data generated by the TCGA Research Network: https://www.cancer.gov/tcga.

This study was supported by grants from the Ragnar Söderberg Foundation, the Swedish Cancer Society, the Swedish Research Council, the Swedish Childhood Cancer Fund, Ollie & Elof Ericssons Foundation, Jeanssons Stiftelser, the Crafoord Foundation, Gösta Miltons Donationsfond, Stiftelsen Cancera, donations from Viveca Jeppson and Maj-Britt and Allan Johansson and the Seve Ballesteros Foundation. J. Bengzon was supported by Region Skane and ALF.

The costs of publication of this article were defrayed in part by the payment of page charges. This article must therefore be hereby marked *advertisement* in accordance with 18 U.S.C. Section 1734 solely to indicate this fact.

Received May 27, 2020; revised November 2, 2020; accepted January 19, 2021; published first January 22, 2021.

References

1. Stupp R, Hegi ME, Mason WP, van den Bent MJ, Taphoorn MJ, Janzer RC, et al. Effects of radiotherapy with concomitant and adjuvant temozolomide versus radiotherapy alone on survival in glioblastoma in a randomised phase III study: 5-year analysis of the EORTC-NCIC trial. Lancet Oncol 2009;10:459–66.
2. Huse JT, Holland EC. Targeting brain cancer: advances in the molecular pathology of malignant glioma and medulloblastoma. Nat Rev Cancer 2010;10:319–31.
3. Hess CF, Schaaf JC, Kortmann RD, Schabet M, Bamberg M. Malignant glioma: patterns of failure following individually tailored limited volume irradiation. Radiother Oncol 1994;30:146–9.
4. Lathia JD, Mack SC, Mulkearns-Hubert EE, Valentim CL, Rich JN. Cancer stem cells in glioblastoma. Genes Dev 2015;29:1203–17.
5. Bao S, Wu Q, McLendon RE, Hao Y, Shi Q, Hjelmeland AB, et al. Glioma stem cells promote radioresistance by preferential activation of the DNA damage response. Nature 2006;444:756–60.
6. Li Z, Bao S, Wu Q, Wang H, Eyler C, Sathornsumetee S, et al. Hypoxia-inducible factors regulate tumorigenic capacity of glioma stem cells. Cancer Cell 2009;15:501–13.
7. Pietras A, Katz AM, Ekstrom EJ, Wee B, Halliday JJ, Pitter KL, et al. Osteopontin-CD44 signaling in the glioma perivascular niche enhances cancer stem cell phenotypes and promotes aggressive tumor growth. Cell Stem Cell 2014;14:357–69.
8. Barnes JM, Kaushik S, Bainer RO, Sa JK, Woods EC, Kai F, et al. A tension-mediated glycocalyx-integrin feedback loop promotes mesenchymal-like glioblastoma. Nat Cell Biol 2018;20:1203–14.

9. Wang X, Prager BC, Wu Q, Kim LJY, Gimple RC, Shi Y, et al. Reciprocal signaling between glioblastoma stem cells and differentiated tumor cells promotes malignant progression. Cell Stem Cell 2018;22:514–28.
10. Hide T, Shibahara I, Kumabe T. Novel concept of the border niche: glioblastoma cells use oligodendrocytes progenitor cells (GAOs) and microglia to acquire stem cell-like features. Brain Tumor Pathol 2019;36:63–73.
11. Calabrese C, Poppleton H, Kocak M, Hogg TL, Fuller C, Hamner B, et al. A perivascular niche for brain tumor stem cells. Cancer Cell 2007;11:69–82.
12. Hambardzumyan D, Bergers G. Glioblastoma: defining tumor niches. Trends Cancer 2015;1:252–65.
13. Quail DF, Joyce JA. The microenvironmental landscape of brain tumors. Cancer Cell 2017;31:326–41.
14. Mega A, Hartmark Nilsen M, Leiss LW, Tobin NP, Miletic H, Sleire L, et al. Astrocytes enhance glioblastoma growth. Glia 2020;68:316–27.
15. Pyonteck SM, Akkari L, Schuhmacher AJ, Bowman RL, Sevenich L, Quail DF, et al. CSF-1R inhibition alters macrophage polarization and blocks glioma progression. Nat Med 2013;19:1264–72.
16. Holland EC, Hively WP, DePinho RA, Varmus HE. A constitutively active epidermal growth factor receptor cooperates with disruption of G1 cell-cycle arrest pathways to induce glioma-like lesions in mice. Genes Develop 1998;12:3675–85.
17. Ozawa T, Riester M, Cheng YK, Huse JT, Squatrito M, Helmy K, et al. Most human non-GCIMP glioblastoma subtypes evolve from a common proneural-like precursor glioma. Cancer Cell 2014;26:288–300.
18. Xie Y, Bergstrom T, Jiang Y, Johansson P, Marinescu VD, Lindberg N, et al. The human glioblastoma cell culture resource: validated cell models representing all molecular subtypes. EBioMedicine 2015;2:1351–63.
19. Bleau AM, Hambardzumyan D, Ozawa T, Fomchenko EI, Huse JT, Brennan CW, et al. PTEN/PI3K/Akt pathway regulates the side population phenotype and ABCG2 activity in glioma tumor stem-like cells. Cell Stem Cell 2009;4:226–35.
20. Naba A, Clauser KR, Hynes RO. Enrichment of extracellular matrix proteins from tissues and digestion into peptides for mass spectrometry analysis. J Vis Exp 2015:e53057. DOI: 10.3791/53057.
21. Hu Y, Smyth GK. ELDA: extreme limiting dilution analysis for comparing depleted and enriched populations in stem cell and other assays. J Immunol Methods 2009;347:70–8.
22. Cancer Genome Atlas Research Network. Comprehensive genomic characterization defines human glioblastoma genes and core pathways. Nature 2008;455:1061–8.
23. Zhao Z, Zhang Kn, Wang Q, Li G, Zeng F, Zhang Y, et al. Chinese Glioma Genome Atlas (CGGA): A Comprehensive Resource with Functional Genomic Data for Chinese Glioma Patients. 2020:2020.01.20.911982.
24. Puchalski RB, Shah N, Miller J, Dalley R, Nomura SR, Yoon JG, et al. An anatomic transcriptional atlas of human glioblastoma. Science 2018;360:660–3.
25. Bowman RL, Wang Q, Carro A, Verhaak RG, Squatrito M. GlioVis data portal for visualization and analysis of brain tumor expression datasets. Neuro Oncol 2017;19:139–41.
26. Carpenter AE, Jones TR, Lamprecht MR, Clarke C, Kang IH, Friman O, et al. CellProfiler: image analysis software for identifying and quantifying cell phenotypes. Genome Biol 2006;7:R100.
27. Pastrana E, Silva-Vargas V, Doetsch F. Eyes wide open: a critical review of sphere-formation as an assay for stem cells. Cell Stem Cell 2011;8:486–98.
28. Chiang CS, McBride WH, Withers HR. Radiation-induced astrocytic and microglial responses in mouse brain. Radiother Oncol 1993;29:60–8.
29. Schneider L, Fumagalli M, d'Adda di Fagagna F. Terminally differentiated astrocytes lack DNA damage response signaling and are radioresistant but retain DNA repair proficiency. Cell Death Differ 2012;19:582–91.
30. Sofroniew MV, Vinters HV. Astrocytes: biology and pathology. Acta Neuropathol 2010;119:7–35.
31. Gong L, Gu J, Ge J, Wu X, Zhang C, Yang C, et al. Differential radiation response between normal astrocytes and glioma cells revealed by comparative transcriptome analysis. OncoTargets Ther 2017;10:5755–64.
32. Condello S, Sima L, Ivan C, Cardenas H, Schiltz G, Mishra RK, et al. Tissue tranglutaminase regulates interactions between ovarian cancer stem cells and the tumor niche. Cancer Res 2018;78:2990–3001.
33. Fu J, Yang QY, Sai K, Chen FR, Pang JC, Ng HK, et al. TGM2 inhibition attenuates ID1 expression in CD44-high glioma-initiating cells. Neuro-oncol 2013;15:1353–65.
34. Yin J, Oh YT, Kim JY, Kim SS, Choi E, Kim TH, et al. Transglutaminase 2 inhibition reverses mesenchymal transdifferentiation of glioma stem cells by regulating C/EBPbeta signaling. Cancer Res 2017;77:4973–84.
35. Deininger MH, Grote E, Wickboldt J, Meyermann R. Distinct radiochemotherapy protocols differentially influence cellular proliferation and expression of p53 and Bcl-2 in glioblastoma multiforme relapses in vivo. J Neurooncol 2000;48:121–9.
36. Anido J, Saez-Borderias A, Gonzalez-Junca A, Rodon L, Folch G, Carmona MA, et al. TGF-beta receptor inhibitors target the CD44(high)/Id1(high) glioma-initiating cell population in human glioblastoma. Cancer Cell 2010;18:655–68.
37. Cooper J, Giancotti FG. Integrin signaling in cancer: mechanotransduction, stemness, epithelial plasticity, and therapeutic resistance. Cancer Cell 2019;35:347–67.
38. Turner PM, Lorand L. Complexation of fibronectin with tissue transglutaminase. Biochemistry 1989;28:628–35.
39. Tang Z, Kang B, Li C, Chen T, Zhang Z. GEPIA2: an enhanced web server for large-scale expression profiling and interactive analysis. Nucleic Acids Res 2019;47:W556–w60.
40. Bouchard G, Therriault H, Bujold R, Saucier C, Paquette B. Induction of interleukin-1β by mouse mammary tumor irradiation promotes triple negative breast cancer cells invasion and metastasis development. Int J Radiat Biol 2017;93:507–16.
41. Desmarais G, Fortin D, Bujold R, Wagner R, Mathieu D, Paquette B. Infiltration of glioma cells in brain parenchyma stimulated by radiation in the F98/Fischer rat model. Int J Radiat Biol 2012;88:565–74.
42. Desmarais G, Charest G, Fortin D, Bujold R, Mathieu D, Paquette B. Cyclooxygenase-2 inhibitor prevents radiation-enhanced infiltration of F98 glioma cells in brain of Fischer rat. Int J Radiat Biol 2015;91:624–33.
43. Li D, Tian Y, Hu Y, Qi Y, Tian N, Li S, et al. Glioma-associated human endothelial cell-derived extracellular vesicles specifically promote the tumourigenicity of glioma stem cells via CD9. Oncogene 2019;38:6898–912.
44. Silver DJ, Lathia JD. Therapeutic injury and tumor regrowth: tumor resection and radiation establish the recurrent glioblastoma microenvironment. EBioMedicine 2018;31:13–4.
45. Jamal M, Rath BH, Williams ES, Camphausen K, Tofilon PJ. Microenvironmental regulation of glioblastoma radioresponse. Clin Cancer Res 2010;16:6049–59.
46. Akkari L, Bowman RL, Tessier J, Klemm F, Handgraaf SM, de Groot M, et al. Dynamic changes in glioma macrophage populations after radiotherapy reveal CSF-1R inhibition as a strategy to overcome resistance. Sci Transl Med 2020;12:eaaw7843.
47. Dyer LM, Schooler KP, Ai L, Klop C, Qiu J, Robertson KD, et al. The transglutaminase 2 gene is aberrantly hypermethylated in glioma. J Neurooncol 2011;101:429–40.
48. Serres E, Debarbieux F, Stanchi F, Maggiorella L, Grall D, Turchi L, et al. Fibronectin expression in glioblastomas promotes cell cohesion, collective invasion of basement membrane in vitro and orthotopic tumor growth in mice. Oncogene 2014;33:3451–62.
49. Giannopoulou E, Katsoris P, Hatziapostolou M, Kardamakis D, Kotsaki E, Polytarchou C, et al. X-rays modulate extracellular matrix in vivo. Int J Cancer 2001;94:690–8.
50. Cordes N, Hansmeier B, Beinke C, Meineke V, van Beuningen D. Irradiation differentially affects substratum-dependent survival, adhesion, and invasion of glioblastoma cell lines. Br J Cancer 2003;89:2122–32.

Cancer Research
The Journal of Cancer Research (1916–1930) | The American Journal of Cancer (1931–1940)

AACR American Association for Cancer Research

The Irradiated Brain Microenvironment Supports Glioma Stemness and Survival via Astrocyte-Derived Transglutaminase 2

Tracy J. Berg, Carolina Marques, Vasiliki Pantazopoulou, et al.

Cancer Res 2021;81:2101-2115. Published OnlineFirst January 22, 2021.